

# Activities, substrate specificity, and genetic interactions of fission yeast Siw14, a cysteinyl-phosphatase-type inositol pyrophosphatase

Ana M. Sanchez,<sup>1,2</sup> Beate Schwer,<sup>3</sup> Nikolaus Jork,<sup>4,5</sup> Henning J. Jessen,<sup>4</sup> Stewart Shuman<sup>1</sup>

**AUTHOR AFFILIATIONS** See affiliation list on p. 16.

**ABSTRACT** Inositol pyrophosphate 1,5-IP<sub>8</sub> is a signaling molecule that regulates phosphate and polyphosphate homeostasis in the fission yeast *Schizosaccharomyces pombe*. 1,5-IP<sub>8</sub> levels are dictated by a balance between the Asp1 kinase domain that converts 5-IP<sub>7</sub> to 1,5-IP<sub>8</sub> and two pyrophosphatases—the Asp1 pyrophosphatase domain (histidine acid phosphatase family) and the Aps1 pyrophosphatase enzyme (Nudix family)—that hydrolyze the β-phosphates of 1,5-IP<sub>8</sub>. Here, we characterize *S. pombe* Siw14 (SpSiw14), a cysteinyl-phosphatase family member and a homolog of *Saccharomyces cerevisiae* Siw14, as a third fission yeast pyrophosphatase implicated in inositol pyrophosphate catabolism. We find that SpSiw14's substrate repertoire embraces inorganic pyrophosphate, inorganic polyphosphate, and the inositol pyrophosphates 5-IP<sub>7</sub>, 1-IP<sub>7</sub>, and 1,5-IP<sub>8</sub>, in addition to the generic substrate *p*-nitrophenylphosphate. Genetic analyses revealed that (i) elimination of the SpSiw14 protein or inactivation of the SpSiw14 pyrophosphatase by the C189S mutation had no effect on *S. pombe* growth but was lethal in the absence of Aps1 and (ii) the synthetic lethality of *siw14Δ aps1Δ* depended on the synthesis of 1,5-IP<sub>8</sub> by the Asp1 kinase. We conclude that SpSiw14 and Aps1 pyrophosphatases have essential but redundant functions in fission yeast, and that their synthetic lethality is a consequence of the toxic effects of too much 1,5-IP<sub>8</sub>. Suppression of *siw14Δ aps1Δ* lethality by loss-of-function mutations of components of the fission yeast 3'-processing/termination machinery fortifies the case for overzealous transcription termination as the basis for 1,5-IP<sub>8</sub> toxicosis.

**IMPORTANCE** The inositol pyrophosphate signaling molecule 1,5-IP<sub>8</sub> modulates fission yeast phosphate homeostasis via its action as an agonist of RNA 3'-processing and transcription termination. Cellular 1,5-IP<sub>8</sub> levels are determined by a balance between the activities of the inositol polyphosphate kinase Asp1 and several inositol pyrophosphatase enzymes. Here, we characterize *Schizosaccharomyces pombe* Siw14 (SpSiw14) as a cysteinyl-phosphatase-family pyrophosphatase enzyme capable of hydrolyzing the phosphoanhydride substrates inorganic pyrophosphate, inorganic polyphosphate, and inositol pyrophosphates 5-IP<sub>7</sub>, 1-IP<sub>7</sub>, and 1,5-IP<sub>8</sub>. Genetic analyses implicate SpSiw14 in 1,5-IP<sub>8</sub> catabolism *in vivo*, insofar as: loss of SpSiw14 activity is lethal in the absence of the Nudix-type inositol pyrophosphatase enzyme Aps1; and *siw14Δ aps1Δ* lethality depends on synthesis of 1,5-IP<sub>8</sub> by the Asp1 kinase. Suppression of *siw14Δ aps1Δ* lethality by loss-of-function mutations of 3'-processing/termination factors points to precocious transcription termination as the cause of 1,5-IP<sub>8</sub> toxicosis.

**KEYWORDS** inositol pyrophosphates, inorganic polyphosphate, pyrophosphatase, *Schizosaccharomyces pombe*, transcription termination

**Editor** Fred M. Winston, Harvard Medical School, Boston, Massachusetts, USA

Address correspondence to Stewart Shuman, shumans@mskcc.org.

The authors declare no conflicts of interest.

See the funding table on p. 16.

**Received** 6 August 2023

**Accepted** 9 August 2023

**Published** 29 September 2023

Copyright © 2023 Sanchez et al. This is an open-access article distributed under the terms of the [Creative Commons Attribution 4.0 International license](https://creativecommons.org/licenses/by/4.0/).

Inositol pyrophosphates IP<sub>7</sub> and IP<sub>8</sub> are signaling molecules that influence eukaryotic phosphate and polyphosphate homeostasis (1). 5-IP<sub>7</sub> and 1-IP<sub>7</sub> differ according to whether the pyrophosphate moiety is at the 1 or 5 position of the inositol ring; 1,5-IP<sub>8</sub> is pyrophosphorylated at both ring positions. 1,5-IP<sub>8</sub> is synthesized from phytic acid (IP<sub>6</sub>) by the sequential action of inositol polyphosphate kinases Kcs1/IP6K, which converts IP<sub>6</sub> to 5-IP<sub>7</sub>, and Asp1/Vip1/VIH/PPIP5K, which converts 5-IP<sub>7</sub> to 1,5-IP<sub>8</sub> (1). Asp1, Vip1, VIH, and PPIP5K—as they are named in fission yeast, budding yeast, plants, and humans, respectively—are bifunctional enzymes composed of an N-terminal kinase domain that synthesizes 1,5-IP<sub>8</sub> and a C-terminal pyrophosphatase domain of the histidine acid phosphatase enzyme family that converts 1,5-IP<sub>8</sub> back to 5-IP<sub>7</sub> (2–8).

In addition to the C-terminal pyrophosphatase domain of Asp1/Vip1/VIH/PPIP5K, two other classes of pyrophosphatases are engaged in the catabolism of inositol pyrophosphates. The first class, exemplified by DIPPP/Ddp1/Aps1 (from human, budding yeast, and fission yeast, respectively), are Nudix-family pyrophosphatases, defined by an ~23 aa Nudix box motif in which three glutamates comprise a binding site for catalytic magnesium ions (9–12). DIPPP/Ddp1/Aps1 are also active in hydrolyzing inorganic polyphosphates and/or diadenosine polyphosphates (12–15).

The founder of the second class of pyrophosphatases is the *Saccharomyces cerevisiae* enzyme Siw14 (ScSiw14), which removes the 5-β-phosphate from 5-IP<sub>7</sub> and 1,5-IP<sub>8</sub> but does not hydrolyze the 1-β-phosphate of 1-IP<sub>7</sub> (16, 17). ScSiw14 (281-aa) belongs to the cysteinyl-phosphatase family of phosphohydrolases, defined by a conserved active site phosphate-binding loop HCxxxxR, that catalyzes phosphoryl transfer to water via a covalent enzyme-(cysteinyl-S<sub>γ</sub>)-phosphate intermediate. Mutating ScSiw14's active site, Cys214, to serine abolishes its activity. Crystal structures of N-terminally deleted versions of ScSiw14 have been solved with sulfate or citrate anions in the active site (17, 18). The plant *Arabidopsis thaliana* encodes five paralogous Siw14 homologs (named PFA-DSPs 1–5) that prefer to hydrolyze the 5-β-phosphate of inositol pyrophosphates (19). Crystal structures of N-terminally truncated plant PFA-DSP1 have been solved, either of wild-type DSP1 with its product inorganic phosphate in the active site or the inactive C150S mutant with its active site filled by its preferred substrate 5-IP<sub>7</sub> (20).

In the fission yeast *Schizosaccharomyces pombe*, IP<sub>8</sub> dynamics are dictated by a balance between Asp1 kinase and the pyrophosphatase enzymes that remove the 1- or 5-β-phosphate groups. *asp1Δ* cells or kinase-inactive *asp1-D333A* mutant cells are viable and contain no detectable 1,5-IP<sub>8</sub> (3, 4). Pyrophosphatase-defective *asp1-H397A* cells are viable but contain elevated levels of 1,5-IP<sub>8</sub> (3, 4). A key finding was that the *asp1-H397A* mutation is synthetically lethal in an *aps1Δ* strain that lacks the Nudix pyrophosphatase enzyme, signifying that too much 1,5-IP<sub>8</sub> is toxic to fission yeast (21). Multiple lines of genetic, biochemical, and transcriptomic evidence cohere to show that (i) 1,5-IP<sub>8</sub> acts as an agonist of precocious RNA polymerase II (Pol2) transcription termination dependent on the 3' cleavage and polyadenylation factor (CPF) complex and (ii) 1,5-IP<sub>8</sub> toxicosis results from overzealous 3'-processing/transcription termination (21–24).

It is not known whether or how Siw14 contributes to 1,5-IP<sub>8</sub> metabolism or 1,5-IP<sub>8</sub> signaling in fission yeast. The present study, in which we interrogate the biochemical activity of *S. pombe* Siw14 (SpSiw14) and its genetic interactions, is inspired by our recent observations that *siw14Δ*, which has no effect *per se* on fission yeast growth, is synthetically lethal with *aps1Δ* (lacking the Nudix-type pyrophosphatase) (25). We report here that SpSiw14 hydrolyzes the generic phosphomonoester *p*-nitrophenylphosphate, the inorganic phosphoanhydride substrates pyrophosphate and polyphosphate, and the inositol pyrophosphates 5-IP<sub>7</sub>, 1-IP<sub>7</sub>, and 1,5-IP<sub>8</sub>. Active site mutation C189S abolishes phosphohydrolase activity *in vitro* and results in lethality with *aps1Δ* *in vivo*. Genetic suppression implicates overzealous 3'-processing/transcription termination as the basis for *siw14Δ* *aps1Δ* lethality.

## RESULTS

Recombinant *S. pombe* Siw14 is a metal-independent phosphohydrolase

We produced recombinant full-length (aa 1–287) wild-type SpSiw14 and a full-length active site mutant C189S in *Escherichia coli* as His<sub>10</sub>Smt3 fusions and isolated them from soluble bacterial extracts by Ni-affinity chromatography. The tags were removed by treatment with the Smt3 protease Ulp1, and the SpSiw14 proteins were recovered free of His<sub>10</sub>Smt3 after a second round of Ni-affinity chromatography. In parallel, we produced and purified N-terminally truncated versions: wild-type SpSiw14-(79–287) and SpSiw14-(79–287)-C189S. The proteins were subjected to a final gel filtration step, during which they eluted as single peaks consistent with monomeric native size. SDS-PAGE revealed comparable purity of the recombinant wild-type and C189S proteins of the expected sizes (Fig. 1A).

To interrogate SpSiw14 enzymatic function, we tested activity with the generic phosphomonoesterase substrate *p*-nitrophenylphosphate. Hydrolysis of *p*-nitrophenylphosphate liberates *p*-nitrophenol, which is quantified by its absorbance at 410 nm. We found that full-length SpSiw14 and truncated SpSiw14-(79–287) readily converted 10 mM *p*-nitrophenylphosphate into *p*-nitrophenol during a 60-min reaction at 37°C in the absence of a divalent cation. Equivalent amounts of SpSiw14-C189S and SpSiw14-(79–287)-C189S were catalytically inert (Fig. 1B).

SpSiw14 *p*-nitrophenylphosphatase was optimal at pH 4.5 to 5.0; activity declined steadily as the pH was increased to 8.0 (Fig. 2A). The extent of *p*-nitrophenylphosphate hydrolysis during a 60-min reaction increased linearly with input full-length SpSiw14 or truncated SpSiw14-(79–287) up to 25 pmol and continued to increase with a shallower slope in the range of 25 to 200 pmol, at which point 70% of the substrate was consumed (Fig. 2B). From the slopes of the SpSiw14 and SpSiw14-(79–287) titration curves in the initial linear phase, we calculated specific activities of 4.9 and 4.3 nmol of *p*-nitrophenol formed per pmol of SpSiw14 and SpSiw14-(79–287), respectively. SpSiw14 activity during a 20-min reaction under steady-state conditions (<10% of substrate consumed by 0.8 μM enzyme) displayed a hyperbolic dependence on *p*-nitrophenylphosphate concentration (Fig. 2C). Fitting the data to the Michaelis-Menten equation yielded  $K_m$  and  $k_{cat}$  values

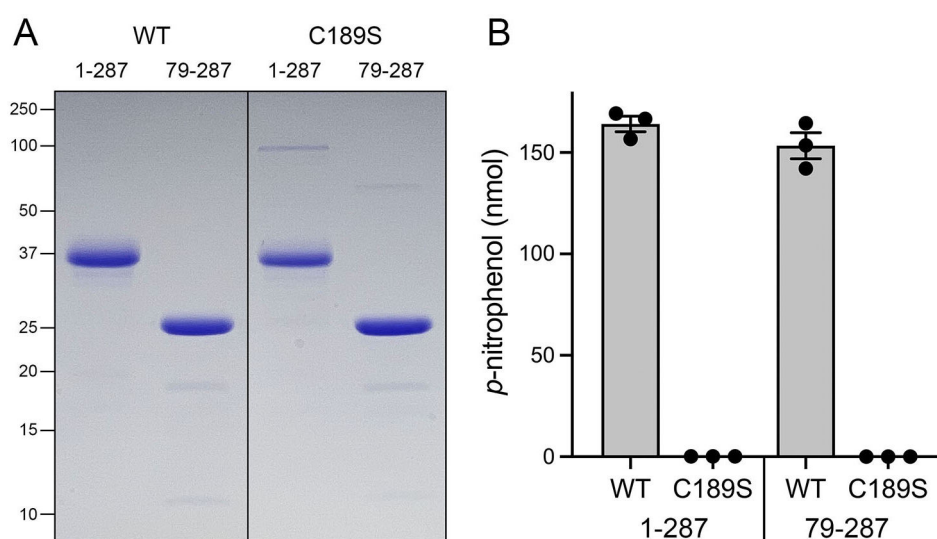


**FIG 1** Recombinant Siw14 hydrolyzes *p*-nitrophenylphosphate. (A) Aliquots (5 μg) of the indicated wild-type or mutant Siw14 preparations were analyzed by SDS-PAGE. The Coomassie blue-stained gel is shown. The positions and sizes (kDa) of marker polypeptides are indicated on the left. (B) Phosphatase reaction mixtures (50 μL) containing 25 mM Tris-acetate, pH 5.0, 1 mM DTT, 10 mM (500 nmol) *p*-nitrophenylphosphate, and 0.8 μM (40 pmol) of the wild-type or mutant Siw14 preparations were incubated at 37°C for 60 min. The extent of *p*-nitrophenol production is plotted. Data in the bar graph are the average of three independent assays ± SEM.

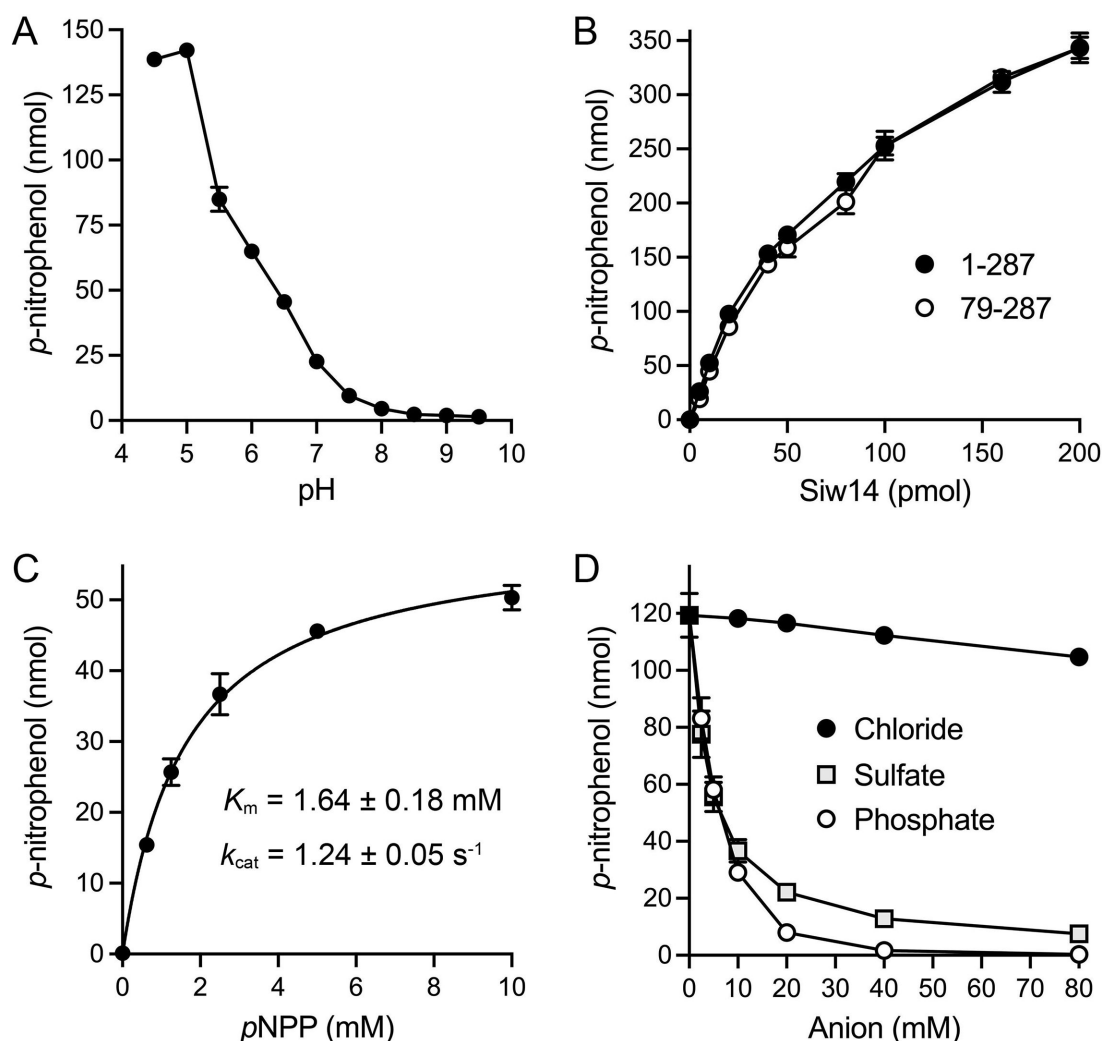


**FIG 2** Characterization of the Siw14 *p*-nitrophenylphosphatase activity. (A) pH profile. Reaction mixtures (50  $\mu$ L) containing 25 mM buffer (either Tris-acetate pH 4.5, 5.0, 5.5, 6.0, 6.5 or Tris-HCl pH 7.0, 7.5, 8.0, 8.5, 9.0, 9.5), 1 mM DTT, 10 mM (500 nmol) *p*-nitrophenylphosphate, and 0.8  $\mu$ M (40 pmol) of Siw14-(1-287) were incubated at 37°C for 60 min. The extent of *p*-nitrophenol production is plotted. Each datum is the average of two independent experiments  $\pm$  range. (B) Siw14-(1-287) and Siw14-(79-287) titration. Reaction mixtures (50  $\mu$ L) containing 25 mM Tris-acetate, pH 5.0, 1 mM DTT, 10 mM (500 nmol) *p*-nitrophenylphosphate, and increasing amounts of Siw14 as specified on the x-axis were incubated at 37°C for 60 min. *p*-Nitrophenol production is plotted as a function of input Siw14. (C) Steady-state kinetic parameters. Reaction mixtures (50  $\mu$ L) containing 25 mM Tris-acetate, pH 5.0, 1 mM DTT, 0.8  $\mu$ M (40 pmol) Siw14-(1-287), and increasing concentrations of *p*-nitrophenylphosphate as specified on the x-axis were incubated at 37°C for 20 min. *p*-Nitrophenol production is plotted as a function of substrate concentration, and the data were fit to the Michaelis-Menten equation in Prism. (D) Inhibition by phosphate. Reaction mixtures (50  $\mu$ L) containing 25 mM Tris-acetate, pH 5.0, 1 mM DTT, 10 mM (500 nmol) *p*-nitrophenylphosphate, and 0.7  $\mu$ M (35 pmol) Siw14-(1-287) were supplemented with sodium chloride, sodium sulfate, or sodium phosphate at the concentrations specified on the x-axis. The reaction mixtures were incubated at 37°C for 60 min. The extent of *p*-nitrophenol production is plotted as a function of added anion concentration. The data plotted in panels B–D are the averages of three independent experiments  $\pm$  SEM.

of  $1.64 \pm 0.18$  mM and  $74.4 \pm 2.7$  min<sup>-1</sup>, respectively. All ensuing experiments were performed with full-length SpSiw14 proteins.

### SpSiw14 activity is inhibited by phosphate and sulfate

We supplemented the standard reaction mixtures containing 10 mM *p*-nitrophenylphosphate with increasing concentrations of sodium phosphate (2.5, 5, 10, 20, 40, and 80 mM). Parallel reactions were supplemented with the equivalent concentrations of sodium chloride or sodium sulfate. Phosphate and sulfate elicited a similar

concentration-dependent inhibition of SpSiw14 phosphatase activity with an  $IC_{50}$  of  $\sim 5$  mM each (Fig. 2D). These results suggest that inorganic phosphate (a reaction product) and sulfate (a mimetic of phosphate) bind to the active site as well as, or better than, the 10 mM *p*-nitrophenylphosphate substrate. Phosphatase activity was inhibited completely at 40 to 80 mM phosphate; at 80 mM sulfate, the residual activity was 6% of the unsupplemented control. By contrast, chloride had relatively little impact, even up to 80 mM, at which point activity was diminished by only 12% compared to the unsupplemented control (Fig. 2D). We also tested whether magnesium affected Siw14 activity by supplementing reaction mixtures with 5, 10, or 20 mM  $MgCl_2$ . The extent of *p*-nitrophenylphosphate hydrolysis in 5, 10, and 20 mM  $MgCl_2$  was 94%, 91%, and 80%, respectively, of the unsupplemented control (not shown).

### SpSiw14 hydrolyzes inorganic pyrophosphate and polyphosphate

SpSiw14 was reacted for 30 min with 2 mM inorganic pyrophosphate ( $PP_i$ ), and the formation of inorganic phosphate ( $P_i$ ) products was determined via colorimetric assay using the Malachite Green reagent. Hydrolysis of  $PP_i$  displayed a bell-shaped dependence on the pH of the reaction mixture. Pyrophosphatase activity was optimal at pH 4.5 to 5.0; activity declined steadily as the pH was decreased to  $\leq 3.0$  or increased to  $\geq 8.0$  (Fig. 3A). The extent of  $PP_i$  hydrolysis was proportional to input SpSiw14 (Fig. 3B). From the slope of the titration curve in the initial linear phase, we calculated a specific activity of 953 pmol of  $P_i$  formed (i.e., 477 pmol of  $PP_i$  hydrolyzed) per pmol of SpSiw14. Pyrophosphatase activity displayed a hyperbolic dependence on  $PP_i$  concentration (Fig. 3C). Fitting the data to the Michaelis-Menten equation yielded a  $K_m$  value of  $1.13 \pm 0.34$  mM  $PP_i$  and an apparent  $k_{cat}$  of  $26.6 \pm 4.9$  min $^{-1}$  with respect to  $PP_i$  consumed per enzyme.

We then reacted SpSiw14 with inorganic polyphosphate with an average linear polymer chain length of 45 (poly- $P_{45}$ ). The products were analyzed by electrophoresis through a 36% polyacrylamide gel, and the polyphosphate chains were visualized by staining the gel with toluidine blue (Fig. 4A). Increasing input SpSiw14 effected a progressive shortening of the polyphosphate chains. Deploying the malachite green

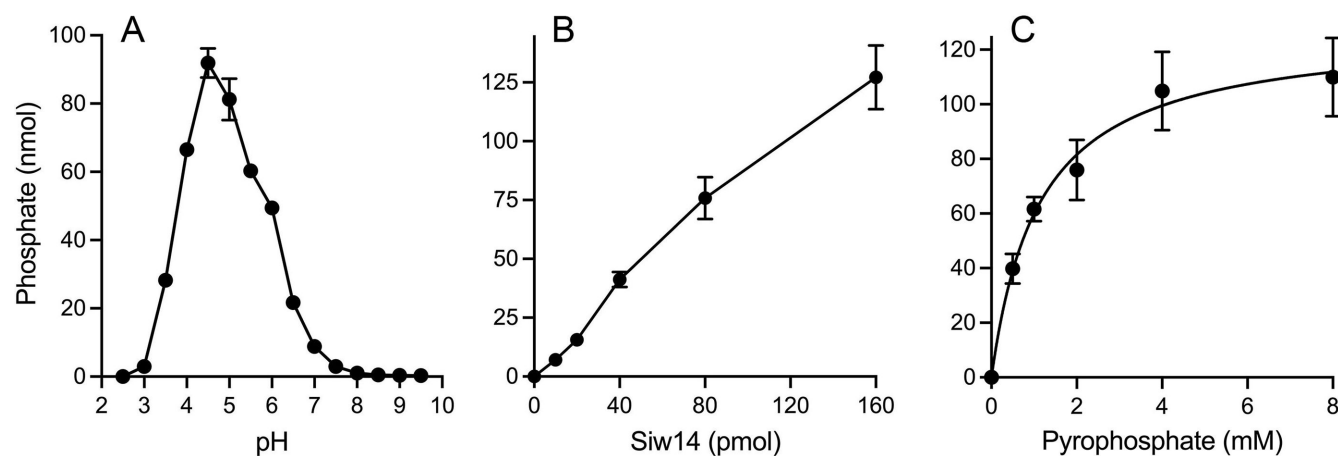


**FIG 3** Siw14 hydrolyzes inorganic pyrophosphate. (A) pH profile. Reaction mixtures (100  $\mu$ L) containing 25 mM buffer (either citric acid pH 2.5, 3.0, 3.5, 4.0; Tris-acetate pH 4.5, 5.0, 5.5, 6.0, 6.5; or Tris-HCl pH 7.0, 7.5, 8.0, 8.5, 9.0, 9.5), 1 mM DTT, 2 mM (200 nmol) sodium pyrophosphate, and 0.8  $\mu$ M (80 pmol) Siw14-(1-287) were incubated at 37°C for 30 min. The extent of phosphate production is plotted as a function of pH. Each datum is the average of two separate titration experiments  $\pm$  range. (B) Siw14 titration. Reaction mixtures (100  $\mu$ L) containing 25 mM Tris-acetate, pH 5.0, 1 mM DTT, 2 mM (200 nmol) sodium pyrophosphate, and increasing amounts of Siw14-(1-287) as specified on the x-axis were incubated at 37°C for 30 min. The extent of phosphate production is plotted. (C) Steady-state kinetic parameters. Reaction mixtures (100  $\mu$ L) containing 25 mM Tris-acetate, pH 5.0, 1 mM DTT, 0.8  $\mu$ M (80 pmol) Siw14-(1-287), and increasing concentrations of sodium pyrophosphate as specified on the x-axis were incubated at 37°C for 30 min. Phosphate production is plotted as a function of pyrophosphate concentration, and the data were fit to the Michaelis-Menten equation in Prism. The data plotted in panels B and C are the averages of three independent experiments  $\pm$  SEM.



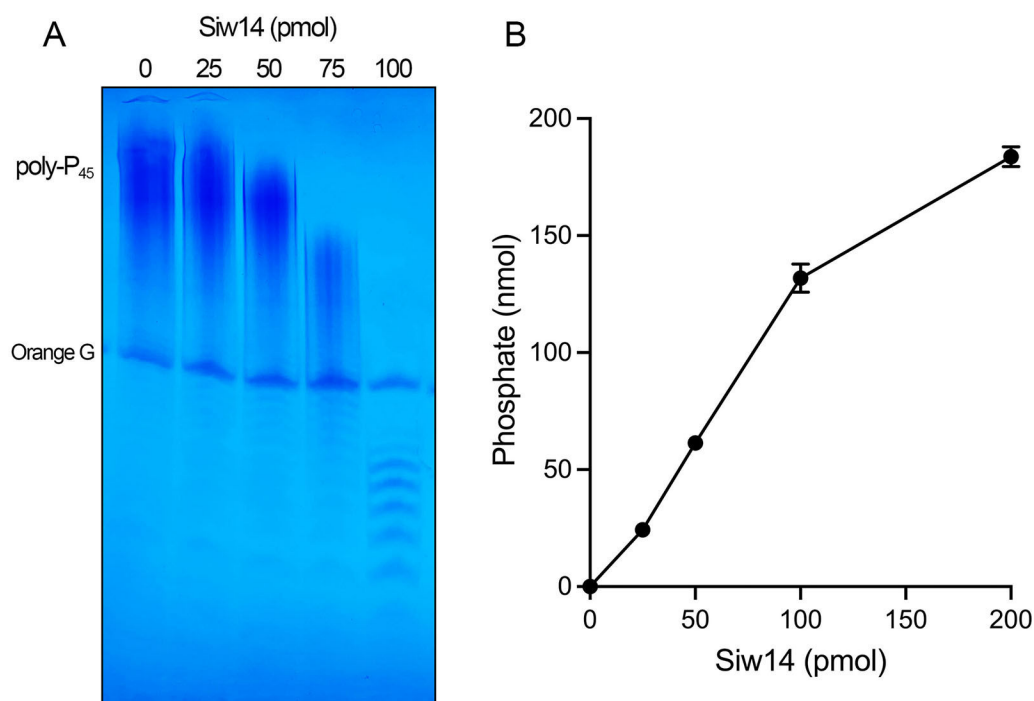


**FIG 4** Siw14 hydrolyzes inorganic polyphosphate. (A) Reaction mixtures (10  $\mu$ L) containing 50 mM Tris-acetate, pH 5.0, 0.2 mM poly-P<sub>45</sub>, and 0, 25, 50, 75, or 100 pmol of Siw14-(1-287) were incubated for 30 min at 37°C. Reaction products were resolved by PAGE and visualized by toluidine blue staining. (B) Reaction mixtures (20  $\mu$ L) containing 50 mM Tris-acetate, pH 5.0, 0.2 mM poly-P<sub>45</sub> (200 nmol total orthophosphate), and increasing concentrations of Siw14(1-287) were incubated for 30 min at 37°C. The extent of orthophosphate production is plotted. The data are the averages of three independent experiments  $\pm$  SEM.

assay, we found that the reaction of SpSiw14 with poly-P<sub>45</sub> generated inorganic phosphate as a reaction product (Fig. 4B). The extent of P<sub>i</sub> release during a 30-min reaction increased with input SpSiw14. At 200 pmol SpSiw14, 92% of the input poly-P was converted to free phosphate. From the slope of the titration curve in the linear range, we calculated that 1.34 nmol of phosphate was released per pmol of SpSiw14, which translates into a turnover number of 45 min<sup>-1</sup>. We conclude that SpSiw14 has vigorous exopolyphosphatase activity.

Poly-P is generated *in vivo* by a heterotrimeric membrane-associated VTC complex (comprising Vtc4, Vtc2, and Vtc1 subunits) that synthesizes poly-P and simultaneously imports the poly-P into the yeast vacuole (26). Poly-P levels and polymer chain length are determined by a dynamic balance between synthesis by the VTC poly-P polymerase and catabolism by exopolyphosphatase or endopolyphosphatase enzymes. *S. pombe* encodes three annotated polyphosphatases: Ppx1, SPBC713.07c, and SPCC1840.07c, of which the latter two are designated as vacuolar. To query whether SpSiw14 contributes significantly to inorganic polyphosphate homeostasis *in vivo*, we monitored the total polyphosphate pool of wild-type and *siw14* $\Delta$  cells (three biological replicates each) via polyacrylamide gel electrophoresis and staining with toluidine blue (Fig. S1). The abundance and length of the linear polyphosphate species were apparently the same in both strains. The lack of impact of *siw14* $\Delta$  on poly-P *in vivo* could simply reflect differential localization, i.e., the cellular poly-P pool is predominantly vacuolar, whereas Siw14 is annotated in Pombase as localizing to the nucleus and cytoplasm.

### SpSiw14 hydrolyzes inositol pyrophosphates

SpSiw14 or SpSiw14-C189S (3.9  $\mu$ M, 78 pmol) was reacted for 60 min with 0.25 mM (5 nmol) 1-IP<sub>7</sub>, 5-IP<sub>7</sub>, or 1,5-IP<sub>8</sub>, and the products were analyzed by electrophoresis

through a 36% polyacrylamide gel. The polyphosphorylated species were visualized by staining the gel with toluidine blue (Fig. 5). Wild-type SpSiw14 effected quantitative conversion of each inositol pyrophosphate substrate to IP<sub>6</sub>. By contrast, SpSiw14-C189S was inert in the hydrolysis of inositol pyrophosphates (Fig. 5). SpSiw14 back-titration (1, 2, and 4 pmol) revealed that 1-IP<sub>7</sub> and 5-IP<sub>7</sub> were hydrolyzed to IP<sub>6</sub> with similar efficiency, and that 1,5-IP<sub>8</sub> was converted to an IP<sub>7</sub> species prior to the formation of the IP<sub>6</sub> end-product (Fig. 6A). Based on the observations that 2 pmol of SpSiw14 sufficed to convert virtually all the input IP<sub>8</sub> (5 nmol) to a mixture of IP<sub>7</sub> and IP<sub>6</sub>, we estimated a turnover number of 83 min<sup>-1</sup> for the SpSiw14 inositol pyrophosphatase, which agrees with the turnover number for hydrolysis of *p*-nitrophenylphosphate.

Our findings here that fission yeast SpSiw14 does not display a marked preference for 5-IP<sub>7</sub> versus 1-IP<sub>7</sub> contrast with the properties reported for *S. cerevisiae* Siw14 (16, 17). In the case of the plant Siw14 homologs, it was found that (i) PFA-DSP1, -DSP2, and -DSP4 hydrolyzed either 5-IP<sub>7</sub> or 1-IP<sub>7</sub> (at 0.33 mM concentration) when the reactions were performed in the absence of a divalent cation and (ii) inclusion of 1 mM magnesium in the reaction mixtures conferred selectivity for 5-IP<sub>7</sub> (19). The selectivity of PFA-DSP1 in the presence of magnesium appears to result from magnesium inhibiting its action on 1-IP<sub>7</sub> but not 5-IP<sub>7</sub> (19). We find that when the enzyme titration experiments were performed in the presence of 1 mM magnesium, SpSiw14 was approximately twofold more active at hydrolyzing 5-IP<sub>7</sub> versus 1-IP<sub>7</sub> (Fig. 6B). Magnesium had no apparent effect on SpSiw14 pyrophosphatase activity with 1,5-IP<sub>8</sub> (Fig. 6A and B).

**siw14-C189S is synthetically lethal with *aps1Δ***

None of the three known fission yeast inositol pyrophosphate pyrophosphatase activities is essential *per se* for vegetative growth, i.e., the pyrophosphatase-defective *asp1-H397A* strain and the *aps1Δ* and *siw14Δ* null strains grow well on yeast extract with supplements (YES) agar at 20°C to 37°C (Fig. 7). However, *asp1-H397A* is synthetically lethal with *aps1Δ* (21), suggesting that simultaneous ablation of these two pyrophosphatases results in the accumulation of toxic levels of 1,5-IP<sub>8</sub>. When attempting to construct a *siw14Δ* *aps1Δ* double mutant strain via mating and sporulation, we found that the *siw14Δ* and *aps1Δ* alleles were synthetically lethal. To wit: (i) we were unable to obtain viable double

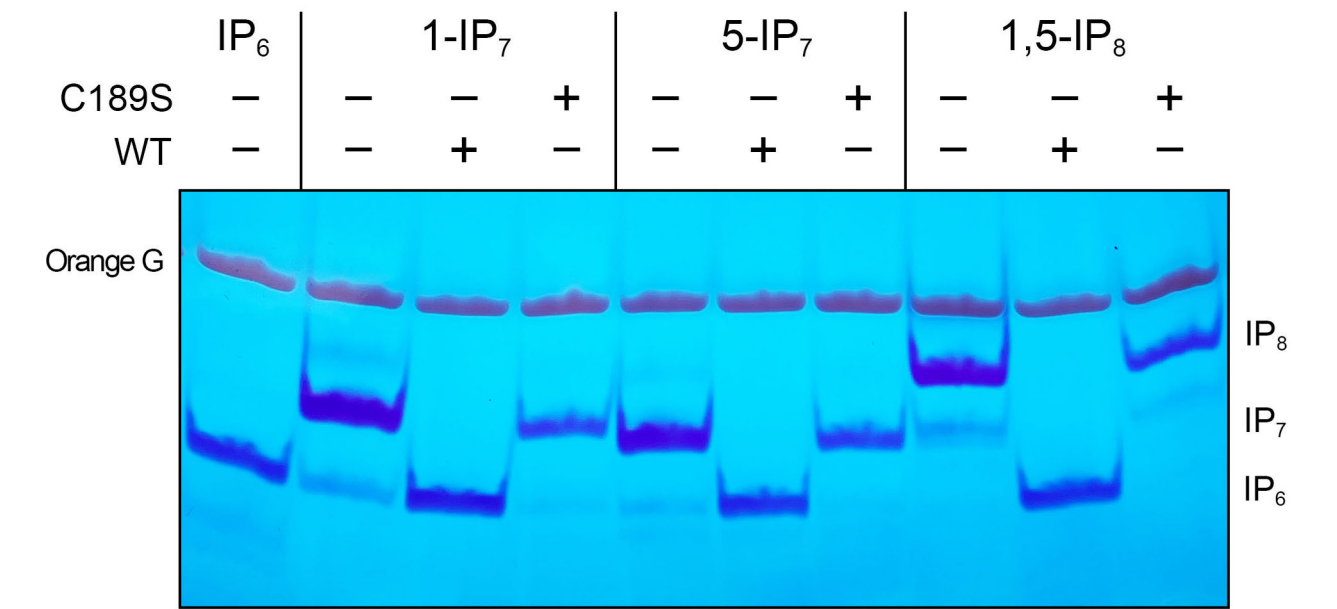


**FIG 5** Siw14 is an inositol pyrophosphate pyrophosphatase. Reaction mixtures (20 μL) containing 30 mM Tris-acetate, pH 5.0, 50 mM NaCl, 0.25 mM (5 nmol) inositol pyrophosphate (1-IP<sub>7</sub>, 5-IP<sub>7</sub>, or 1,5-IP<sub>8</sub>), and 3.9 μM (78 pmol) wild-type or C189S Siw14-(1-287) (where indicated by +) were incubated for 60 min at 37°C. The reaction products were resolved by PAGE and visualized by toluidine blue staining.

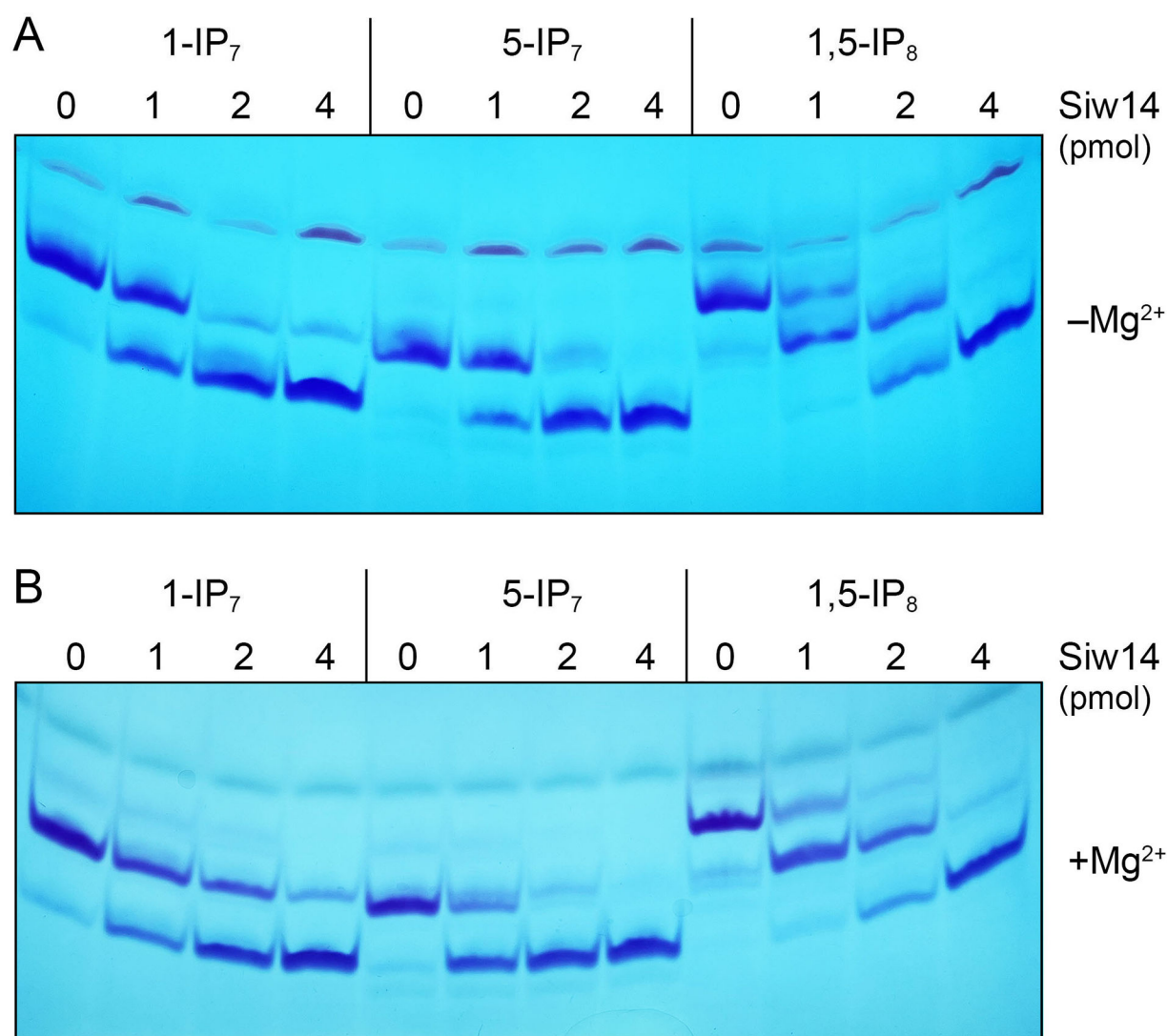


**FIG 6** Siw14 hydrolyzes the 1- $\beta$  and 5- $\beta$  phosphate groups with similar efficiency. Reaction mixtures (10  $\mu$ L) containing 30 mM Tris-acetate, pH 5.0, 25 mM NaCl, 0.5 mM (5 nmol) inositol pyrophosphate (1-IP<sub>7</sub>, 5-IP<sub>7</sub>, or 1,5-IP<sub>8</sub>), in the absence (panel A) or presence of 1 mM MgCl<sub>2</sub> (panel B), and increasing concentrations of wild-type Siw14 as specified were incubated for 30 min at 37°C. The reaction products were resolved by PAGE and visualized by toluidine blue staining.

mutants after screening a large population of haploid progeny of the genetic cross; and (ii) wild-type progeny and the differentially marked *siw14* $\Delta$  (on chromosome II) and *aps1* $\Delta$  (on chromosome I) single mutants were recovered at the expected frequencies (25). This result signified that the SpSiw14 and the Aps1 pyrophosphatases have essential but redundant functions in fission yeast. By contrast, we readily isolated a *siw14* $\Delta$  *aps1-H397A* double mutant that grew as well as wild type on YES agar at all temperatures (Fig. 7).

To see if SpSiw14 pyrophosphatase activity is pertinent to the synthetic lethality of *siw14* $\Delta$  with *aps1* $\Delta$ , we crossed the marked *siw14-C189S* and *aps1* $\Delta$  strains and screened for double-mutants by random spore analysis. The *siw14-C189S* active site mutant phenocopied *siw14* $\Delta$  with respect to synthetic lethality with *aps1* $\Delta$  (Fig. 7), consistent with the idea that inactivation of these two pyrophosphatases at once results in the accumulation of toxic levels of 1,5-IP<sub>8</sub> and/or another phosphoanhydride-containing metabolite.



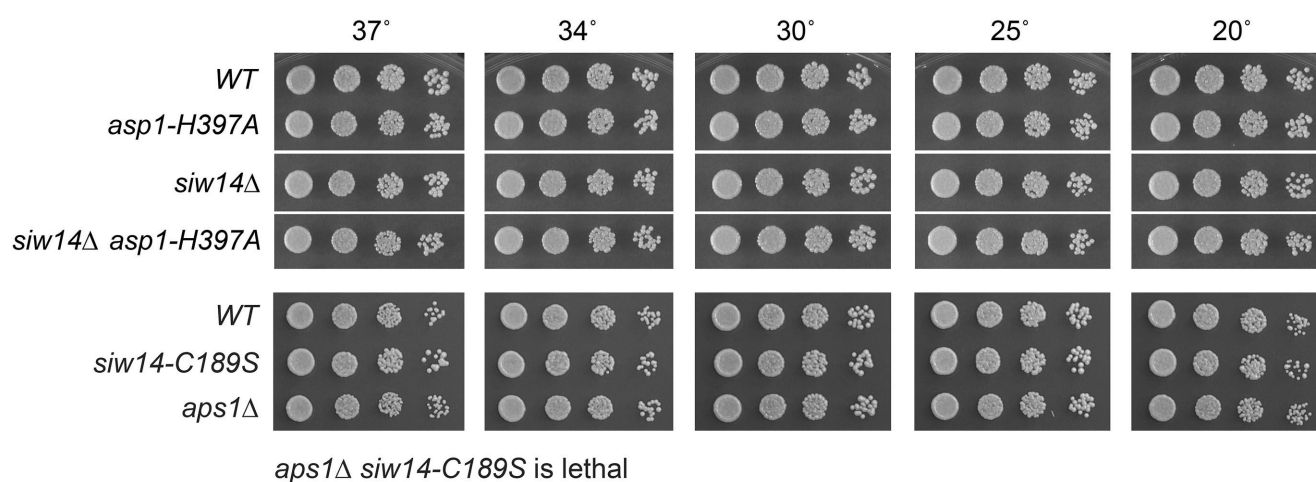


**FIG 7** *siw14-C189S* is synthetically lethal with *aps1Δ*. *S. pombe* strains with the indicated *asp1*, *siw14*, and *aps1* alleles were inoculated in YES broth and grown at 30°C. Exponentially growing cultures were adjusted to an  $A_{600}$  of 0.1, and aliquots (3  $\mu$ L) of serial fivefold dilutions were spotted on YES agar and then incubated at the temperatures specified. *aps1Δ* was synthetically lethal with *siw14-C189S*.

### The lethality of *siw14Δ aps1Δ* depends on Asp1 kinase activity

If the synthetic lethality of *siw14Δ aps1Δ* is due to 1,5-IP<sub>8</sub> toxicity, then the lethality should be suppressed by the kinase-dead *asp1-D333A* allele (6, 8). Indeed, after crossing *aps1Δ asp1-D333A* and *siw14Δ* strains and random spore analysis, we obtained viable *siw14Δ aps1Δ asp1-D333A* cells that grew as well as wild type on YES agar (Fig. 8).

### The lethality of *siw14Δ aps1Δ* depends on CPF subunits, Rhn1, Pin1, and the Pol2 carboxy-terminal domain threonine-4

The fission yeast CPF is a 13-subunit protein assembly responsible for the 3' processing of nascent Pol2 transcripts that precedes and abets Pol2 transcription termination (27). Five of the CPF subunits (Ctf1, Ssu72, Dis2, Ppn1, and Swd22) are dispensable for growth. Dis2 and Ssu72 are phosphoprotein phosphatase enzymes. Rhn1 is an inessential Pol2 termination factor that recognizes the Thr4-PO<sub>4</sub> mark on the carboxy-terminal domain

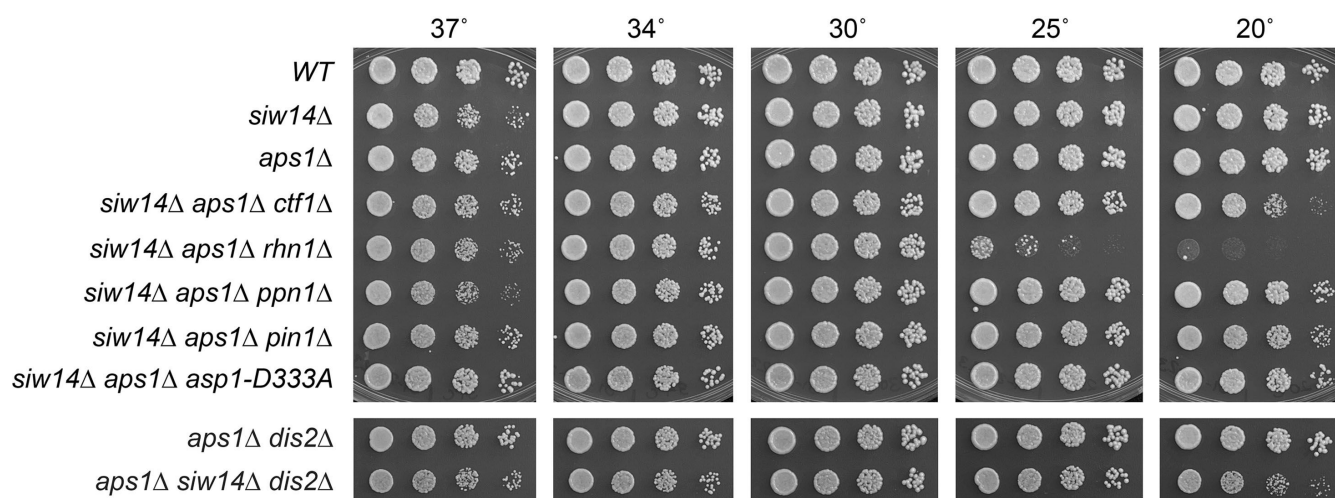


**FIG 8** Lethality of *siw14Δ aps1Δ* depends on Asp1 kinase activity, CPF subunits Ctf1, Dis2, and Ppn1, prolyl isomerase Pin1, and termination factor Rhn1. Fission yeast strains with the *siw14Δ* allele in various combinations with *aps1Δ* and CPF subunit mutations or the Asp1 kinase-inactivating mutation D333A were spot tested for growth at the temperatures specified.

(CTD) of the Rpb1 subunit of Pol2 (28). Pin1 is a peptidyl prolyl isomerase that abets the function of Ssu72, a *cis*-proline-dependent CTD phosphatase (29).

A key question is whether the lethality of the *siw14Δ aps1Δ* strain arises from unconstrained precocious transcription termination caused by too much 1,5-IP<sub>8</sub>. If so, then it might be expected that the lethality would be ameliorated by mutations in the 3'-processing/termination machinery. To test this idea, we crossed our series of *aps1Δ* CPF/*pin1/rhn1* double-mutants to *siw14Δ* then sporulated the resulting diploids and screened random spores for each of the differentially marked loci of interest. In this way, we recovered viable *siw14Δ aps1Δ ctf1Δ*, *siw14Δ aps1Δ swd22Δ*, *siw14Δ aps1Δ ppn1Δ*, *siw14Δ aps1Δ pin1Δ*, *siw14Δ aps1Δ dis2Δ*, and *siw14Δ aps1Δ ssu72-C13S* haploid strains that grew like wild type on YES agar at 25°C, 30°C, and 34°C and, in some cases, grew slowly at 37°C or 20°C, as gauged by colony size (Fig. 8 and 9). The viable *siw14Δ aps1Δ rhn1Δ* triple mutant grew well at 30°C–37°C but displayed a severe cold-sensitive growth defect at 20°C and 25°C (Fig. 8). These results suggest that the synthetic lethality of *siw14Δ aps1Δ* is a consequence of IP<sub>8</sub>-driven precocious termination that depends on CPF, Pin1, and Rhn1.

We tested if *rpb1-CTD-T4A*, which negatively affects 3'-processing/termination (22, 30), would also suppress the lethality of *siw14Δ aps1Δ*. After crossing *aps1Δ CTD-T4A* and *siw14Δ* strains and random spore analysis, we obtained viable triple mutant *siw14Δ aps1Δ CTD-T4A* cells that grew on YES agar at 30°C to 37°C but were severely sick at 25°C and 20°C (Fig. 9).

### *siw14Δ aps1Δ* lethality depends on Spx1

Deleting the inositol pyrophosphate-binding RING-domain ubiquitin ligase Spx1 (or alanine mutations of its inositol pyrophosphate-binding site or zinc-binding cysteines) suppresses the 1,5-IP<sub>8</sub> toxicosis of *asp1* alleles *STF6* and *STF9* (24). Spx1 is proposed to be a mediator of the inositol pyrophosphate signal that leads to precocious transcription termination. Here, we found by crossing *aps1Δ spx1Δ* and *siw14Δ* that *spx1Δ* suppressed the synthetic lethality of *siw14Δ aps1Δ*, such that the *siw14Δ aps1Δ spx1Δ* triple mutant grew as well as wild type on YES agar at all temperatures (Fig. 9).

### Transcriptome profiling of *siw14Δ* cells and comparison to *aps1Δ*

We performed RNA-seq on poly(A)<sup>+</sup> RNA isolated from *siw14Δ* cells and from the parental wild-type strain. cDNAs obtained from three biological replicates (using RNA from cells grown to mid-log phase in YES medium at 30°C) were sequenced for each strain. In the data sets, 86%–88% of the sequence reads were mapped to unique genomic loci (Table S1). Read densities (RPKM) for individual genes were highly reproducible between biological replicates (Pearson coefficients of 0.968 to 0.984) (Table S2). A cutoff of  $\pm 2$ -fold change in normalized transcript read level and an adjusted *P*-value of  $\leq 0.05$  were the criteria applied to derive an initial list of differentially expressed annotated loci in the

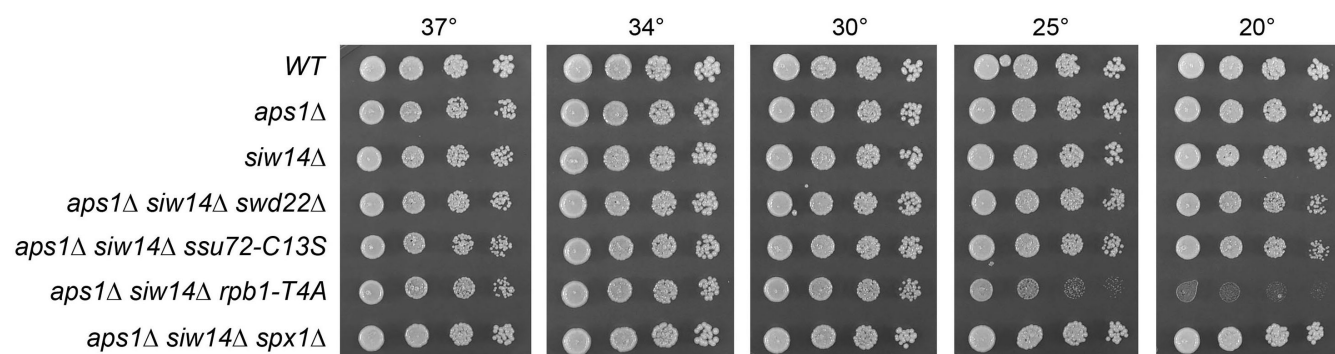


**FIG 9** Lethality of *siw14Δ aps1Δ* depends on CPF subunits Swd22 and Ssu72, CTD threonine-4, and Spx1. *siw14Δ*, *aps1Δ*, and the indicated triple-mutant progeny of genetic crosses were spot-tested for growth on YES agar at the temperatures specified.

*siw14Δ* mutant versus the wild-type control. We then focused on differentially expressed genes with average normalized read counts  $\geq 100$  in either the *siw14Δ* or wild-type strains to eliminate polyadenylated transcripts that were expressed at very low levels in vegetative cells. We thereby identified only 2 annotated protein-coding RNAs that were upregulated and 10 protein-coding RNAs (other than the *siw14* mRNA) that were downregulated in *siw14Δ* cells (Table S3). We surmise that Siw14 has little impact on gene expression in an otherwise wild-type cell.

Our prior RNA-seq analysis of *aps1Δ* cells highlighted 19 coding genes that were upregulated, including *pho1*, *pho84*, and *tgp1* that comprise the *PHO* regulon (21). Expression of the *PHO* genes in phosphate-replete cells is repressed by upstream lncRNA-mediated transcription interference. Derepression of *pho1* mRNA and Pho1 acid phosphatase enzyme activity is a sensitive indicator of genetic mutations that elicit precocious termination of upstream *pri* lncRNA transcription. The present finding by RNA-seq that the *PHO* genes were unaffected in *siw14Δ* cells resonates with our previous observation that *siw14Δ* had no effect on the level of cell-surface Pho1 acid phosphatase activity (25). In *aps1Δ* cells, 28 genes were downregulated, including 4 genes of the iron homeostasis regulon (*frp1*, *fip1*, *fio1*, and *srx1*). The noteworthy overlap between the *siw14Δ* and *aps1Δ* transcriptome data sets was that 6 of the 10 genes downregulated in *siw14Δ* were also downregulated in *aps1Δ*: these being *frp1* (ferric-chelate reductase), *mei2* (RNA binding protein), *SPAC15E1.02c* (DUF1761 family protein), *SPAC637.03* (DUF1774 family protein), *SPCC70.08c* (methyltransferase), and *SPAC26H5.09c* (oxidoreductase involved in NADPH regeneration) (Table S3).

## DISCUSSION

The results herein illuminate the biochemical activities and genetic interactions of the fission yeast pyrophosphatase SpSiw14. The 287-aa SpSiw14 protein is predicted to consist of a disordered N-terminal 80-aa segment fused to a cysteinyl-phosphatase enzyme fold ([alphafold.ebi.ac.uk/entry/Q9UUF3](https://alphafold.ebi.ac.uk/entry/Q9UUF3)). Our initial purification and characterization of recombinant SpSiw14 proteins established its activity as a metal-independent *p*-nitrophenylphosphatase that is strictly dependent on the active site Cys189 thiol but unaffected by deletion of the disordered N-terminus, which has no primary structure similarity to the dispensable N-terminal segment of *S. cerevisiae* Siw14 (17) or the N-terminus of *Arabidopsis* PFA-DSP1. The catalytic domain of SpSiw14 is, by alignment of its primary structure (Fig. S2) and its predicted tertiary structure, highly similar to the crystal structures of ScSiw14 and plant PFA-DSP1 (17, 18, 20). SpSiw14 has a C-terminal peptide extension not found in the other two enzymes, of which the last 18-aa are predicted to be disordered (Fig. S2). The ensuing biochemical analysis of SpSiw14 reported here was performed with the full-length enzyme.

The salient findings were that SpSiw14 has a broader spectrum of pyrophosphatase activities than had been reported in previous studies of yeast and plant enzymes, whereby SpSiw14's substrate repertoire embraces inorganic pyrophosphate, inorganic polyphosphate, and the inositol pyrophosphates 5-IP<sub>7</sub>, 1-IP<sub>7</sub>, and 1,5-IP<sub>8</sub>, in addition to the generic substrate *p*-nitrophenylphosphate. The turnover numbers for these phospho-substrates, derived from steady-state kinetics or estimated from enzyme-specific activity, were similar: 74 min<sup>-1</sup> for *p*-nitrophenylphosphate; 27 min<sup>-1</sup> for inorganic pyrophosphate; 45 min<sup>-1</sup> for inorganic polyphosphate; and 83 min<sup>-1</sup> for 1,5-IP<sub>8</sub>. The reaction rates of SpSiw14 are in the same range as the *k*<sub>cat</sub> values reported for ScSiw14: 79 min<sup>-1</sup> for 5-IP<sub>7</sub> and 38 min<sup>-1</sup> for IP<sub>8</sub> (17).

SpSiw14 activity displays a bell-shaped pH profile with optimal activity at pH 4.5 to 5.0, a steep fall-off at lower pH, and a somewhat more gradual decline at higher pH. This profile suggests the involvement of at least two essential pH-sensitive moieties in the catalytic mechanism, which need to be deprotonated and protonated, respectively. One of these is the active site cysteine-189 that, as a deprotonated thiolate, attacks the terminal phosphate of the substrate to form an enzyme—(cysteinyl-Sγ)-phosphate intermediate. Studies of *Yersinia* PTPase (a founder of the cysteinyl-phosphatase family)

documented an acidic pH optimum (pH 5.0) for *p*-nitrophenylphosphate hydrolysis and a  $pK_a$  of 4.67 for the active site cysteine thiol (31, 32), which is significantly lower than the expected cysteine  $pK_a$  of 8.5. Ensuing crystal structures of many cysteinyl-phosphatase family members led to the insight that the cysteine thiolate is stabilized by a surrounding network of hydrogen bond donors provided by a threonine side chain and several main-chain amides of the active site phosphate-binding loop HCxxxxxRT. As to the nature of the Siw14 moiety that needs to be protonated, we can speculate that this might be a conserved histidine in the Siw14-specific phosphate-binding loop HCxRGKHRT (Fig. S2). This histidine engages in two hydrogen bonds between N $\delta$  and N $\epsilon$  in the ligand-bound structures of the plant Siw14-type phosphatase (20). However, deprotonation of this histidine might not account for the virtually total loss of SpSiw14 phosphatase activity at alkaline pH, insofar as an alanine mutation of the corresponding histidine in ScSiw14 elicited only a fivefold decrement in pyrophosphatase activity with 5-IP<sub>7</sub> (17). Changing this histidine to aspartate in the plant enzyme resulted in a 20-fold decrease in pyrophosphatase activity with 5-IP<sub>7</sub> (20).

SpSiw14 is sensitive to product inhibition by inorganic phosphate in the low millimolar range and is similarly sensitive to inhibition by sulfate. The initially reported *p*-nitrophenylphosphatase activity of recombinant *S. cerevisiae* Siw14, purified as a GST-tagged fusion protein, was notable for its very low apparent  $k_{cat}$  of  $4.4 \times 10^{-7} \text{ s}^{-1}$  (16), which is slower than the presently reported  $k_{cat}$  of  $1.24 \text{ s}^{-1}$  for SpSiw14. While the low turnover was potentially attributed to a high fraction of catalytically inactive protein in the preparation, the enzyme assays in the initial study were conducted in the presence of 10 mM magnesium sulfate (16) and thus likely prone to sulfate inhibition. Changing the expression vector and purification procedures—and, coincidentally, the elimination of sulfate from the enzyme reaction mixtures—resulted in a much more active recombinant *S. cerevisiae* Siw14 preparation that was used by Wang and colleagues for structural and functional studies (17).

Inhibition of Siw14 by inorganic phosphate has potential relevance for fission yeast IP<sub>8</sub> dynamics *in vivo*. 1,5-IP<sub>8</sub> is synthesized *in vivo* from 5-IP<sub>7</sub> by the N-terminal kinase domain of the bifunctional kinase-pyrophosphatase Asp1 (3, 4). *In vitro*, recombinant full-length Asp1 catalyzes futile cycles of 1-phosphate phosphorylation by its kinase component and 1-pyrophosphate hydrolysis by its pyrophosphatase component that result in unproductive consumption of the ATP substrate (5). An H397A mutation in the active site of the C-terminal pyrophosphatase domain of Asp1 restored net 1,5-IP<sub>8</sub> synthesis by full-length Asp1-H397A to nearly the same specific activity as the isolated Asp1 kinase domain. Inspired by studies of the human ortholog PPIP5K2 (7), Benjamin et al. (5) found that inorganic phosphate, the product of the Asp1 inositol pyrophosphate pyrophosphatase reaction, enables net 1,5-IP<sub>8</sub> synthesis *in vitro* by full-length wild-type Asp1. Significant activation of 1,5-IP<sub>8</sub> synthesis was evident at 25 mM phosphate, which is the reported physiological intracellular concentration of orthophosphate in budding yeast grown in phosphate-replete medium (33). Although these findings regarding phosphate's effect on Asp1 pyrophosphatase *in vitro* provided a simple explanation for how Asp1 might achieve net 1,5-IP<sub>8</sub> synthesis in the cellular milieu, the present study injects phosphate-sensitive control of SpSiw14 into the mix. To wit, intracellular phosphate levels sufficient to modulate SpSiw14's inositol pyrophosphatase activities could increase the 5-IP<sub>7</sub> substrate available to Asp1 and reduce turnover of the 1,5-IP<sub>8</sub> product.

The present genetic analyses of fission yeast Siw14 are consistent with it playing a role in 1,5-IP<sub>8</sub> catabolism *in vivo*, insofar as: (i) elimination of Siw14 protein or inactivation of the Siw14 pyrophosphatase by the C189S mutation had no effect *per se* on *S. pombe* growth but was lethal in the absence of the Nudix-type inositol pyrophosphate pyrophosphatase enzyme Aps1; and (ii) the synthetic lethality of *siw14Δ aps1Δ* depended on the synthesis of 1,5-IP<sub>8</sub> by the Asp1 kinase. We conclude that SpSiw14 and the Aps1 pyrophosphatases have essential but redundant functions in fission yeast, and that their synthetic lethality is a consequence of the toxic effects of too much 1,5-IP<sub>8</sub>. Copious



genetic evidence points to 1,5-IP<sub>8</sub> action as an agonist of precocious 3'-processing/transcription termination as the basis for 1,5-IP<sub>8</sub> toxicosis (21–24). We surmise that this is also the case for *siw14Δ aps1Δ* synthetic lethality, which was consistently suppressed by loss-of-function mutations of components of the fission yeast 3'-processing/termination machinery. RNA analyses and monitoring of *PHO* gene expression indicate that the *aps1Δ* deletion leads to increased expression of *pho1* by relieving flanking lncRNA-mediated transcription interference with the *pho1* promoter via precocious lncRNA termination. By contrast, the *siw14Δ* deletion does not elicit such a phenotype on its own. An outstanding challenge is to pinpoint the gene(s) dysregulated by excess 1,5-IP<sub>8</sub> in *siw14Δ aps1Δ* and other lethal IP<sub>8</sub> pyrophosphatase mutants (21, 22) that are responsible for toxicity.

## MATERIALS AND METHODS

### Recombinant *S. pombe* Siw14

The ORF encoding full-length Siw14 was PCR amplified from *S. pombe* cDNA with primers that introduced a BamHI site immediately flanking the start codon and a XhoI site downstream of the stop codon. A truncated ORF encoding Siw14-(79-287) was generated by PCR amplification with a sense-strand primer that introduced a BamHI site overlying the codon for Ser79. The PCR products were digested and inserted between the BamHI and XhoI sites of pET28b-His<sub>10</sub>Smt3 to generate T7 RNA polymerase-based expression plasmids encoding the Siw14-(1-287) and Siw14-(79-287) polypeptides fused to an N-terminal His<sub>10</sub>Smt3 tag. A missense Cys189Ser mutation was introduced into the expression plasmids by two-stage overlap extension PCR with mutagenic primers. All plasmid inserts were sequenced to verify the fusion junctions and exclude the presence of unwanted mutations.

Wild-type and mutant pET28b-His<sub>10</sub>Smt3-Siw14 plasmids were transfected into *E. coli* BL21(DE3) cells. Cultures (1 L) amplified from single kanamycin-resistant transformants were grown at 37°C in Terrific Broth containing 50 µg/mL kanamycin until the A<sub>600</sub> reached 0.72–0.78. The cultures were chilled on ice for 1 h, adjusted to 2.2% (vol/vol) ethanol and 0.5 mM isopropyl-β-D-thiogalactopyranoside, and then incubated for 16 h at 17°C with constant shaking. The cells were harvested by centrifugation and stored at –80°C. All subsequent steps were performed at 4°C. Thawed cells were resuspended in 25 mL of buffer L (50 mM Tris-HCl, pH 7.5, 500 mM NaCl, 25 mM imidazole, 10% glycerol) and half a tablet of cOmplete EDTA-free Protease Inhibitor Cocktail (Roche). The cells were lysed by sonication, and the insoluble material was removed by centrifugation at 38,000 × *g* for 30 min. The supernatant was mixed for 1 h with 3 mL of nickel-nitrilotriacetic acid (Ni-NTA) agarose resin (Qiagen) that had been equilibrated with buffer L. The resin was recovered by centrifugation and washed twice with 30 mL of buffer L. The resin was centrifuged again, resuspended in 15 mL of buffer L, and poured into a column. After washing the column with 15 mL of buffer L, the bound material was eluted with 6 mL of buffer L containing 300 mM imidazole. The polypeptide compositions of the flow-through and eluate fractions were monitored by SDS-PAGE. The 300 mM imidazole eluate fractions containing His<sub>10</sub>-Smt3-Siw14 were supplemented with Smt3-specific protease Ulp1 [Ulp1/His<sub>10</sub>-Smt3-Siw14 ratio of 1:425 (wt/wt)] and then dialyzed overnight against 2 L of buffer D (50 mM Tris-HCl, pH 7.5, 250 mM NaCl, 25 mM imidazole, 5% glycerol). The dialysates were mixed for 1 h with 3 mL of Ni-NTA agarose resin that had been equilibrated with buffer D. Tag-free Siw14 proteins were recovered in the flow-through fractions. Protein concentration was determined from the A<sub>280</sub> measured with a Nanodrop spectrophotometer (Thermo Scientific), applying a molar extinction coefficient of 24,910 M<sup>–1</sup>/cm for full-length Siw14 and 24,660 M<sup>–1</sup>/cm for Siw14-(79-287), as calculated by ProtParam. The yields at this purification step of Siw14-(1-287), Siw14-(1-287)-C189S, Siw14-(79-287), and Siw14-(79-287)-C189S were 12, 20, 16, and 34 mg per liter of bacterial culture, respectively. The tag-free Siw14 preparations were concentrated by centrifugal ultrafiltration (Amicon Ultra-15; 10 kDa cutoff) to 8–14 mg/mL (in a 2-mL volume) and then further purified by gel-filtration through



a 125-mL 16/60 HiLoad Superdex 200 column (GE Healthcare) equilibrated in buffer containing 20 mM Tris-HCl, pH 7.5, 100 mM NaCl, and 2 mM dithiothreitol (DTT) at a flow rate of 0.5 mL/min while collecting 2 mL fractions. The peak Siw14 fractions were pooled and concentrated by centrifugal ultrafiltration (Amicon Ultra-15; 10 kDa cutoff) to 2.5–10 mg/mL. Protein concentration was determined from the  $A_{280}$  measured with a Nanodrop spectrophotometer, applying molar extinction coefficients as described above.

### ***p*-Nitrophenylphosphatase activity**

Reaction mixtures (50  $\mu$ L) containing 25 mM Tris-acetate, pH 5.0, 1 mM DTT, 10 mM (500 nmol) *p*-nitrophenylphosphate, and Siw14 protein as specified in the figure legends were incubated at 37°C. The reactions were quenched by adding 0.95 mL of 1 M Na<sub>2</sub>CO<sub>3</sub>. Release of *p*-nitrophenol was determined by measuring  $A_{410}$  and interpolating the value to a *p*-nitrophenol standard curve.

### **Inorganic pyrophosphatase activity**

Reaction mixtures (100  $\mu$ L) containing 25 mM Tris-acetate, pH 5.0, 1 mM DTT, 2 mM (200 nmol) sodium pyrophosphate, and Siw14 protein as specified in the figure legends were incubated at 37°C. The reactions were quenched by adding 1 mL of Malachite Green Reagent (Enzo Life Sciences), followed by a 20-min incubation at room temperature. Phosphate release was determined by measuring  $A_{620}$  and interpolating the value to a phosphate standard curve.

### **Inorganic polyphosphatase activity**

Reaction mixtures (10  $\mu$ L) containing 50 mM Tris-acetate, pH 5.0, 0.2 mM poly-P<sub>45</sub> (Sigma, Cat # S4379-500MG, Lot # SLBX2788), and Siw14 protein as specified in the figure legends were incubated for 30 min at 37 °C. Reactions were terminated by mixing with an equal volume of 2× Orange G loading buffer (10 mM Tris-HCl, pH 7.0, 1 mM EDTA, 30% glycerol, 0.05% Orange G). The products were analyzed by electrophoresis at 4°C through a 20-cm 36% polyacrylamide gel containing 80 mM Tris-borate (pH 8.3) and 1 mM EDTA for 2.5 h at 10 W constant power. The gel was washed briefly with water and then stained with a solution of 0.1% toluidine blue (Sigma), 20% methanol, and 0.2% glycerol, followed by destaining in 20% methanol.

Alternatively, reaction mixtures (20  $\mu$ L) containing 50 mM Tris-acetate, pH 5.0, 0.2 mM poly-P<sub>45</sub> (Sigma, Cat # S4379-500MG, Lot # SLCM4102), and Siw14 protein as specified in the figure legends were incubated for 30 min at 37°C. Reactions were quenched by adding 1 mL of Malachite Green Reagent (Enzo Life Sciences), followed by a 20-min incubation at room temperature. Phosphate release was determined by measuring  $A_{620}$  and interpolating the value to a phosphate standard curve. The total phosphate content of the poly-P<sub>45</sub> substrate was measured after digestion for 30 min at 37°C with calf intestine alkaline phosphatase (40 U; NEB).

### **Inositol pyrophosphate pyrophosphatase activity**

Reaction mixtures containing 30 mM Tris-acetate, pH 5.0, 25 or 50 mM NaCl, 0.25 or 0.5 mM inositol pyrophosphate (1-IP<sub>7</sub>, 5-IP<sub>7</sub>, or 1,5-IP<sub>8</sub>), 0 or 1 mM MgCl<sub>2</sub>, and Siw14 protein as specified in the figure legends were incubated for 30 min at 37°C. The reactions were terminated by adding an equal volume of 2× Orange G loading buffer. The products were analyzed by electrophoresis at 4°C through a 20-cm 36% polyacrylamide gel containing 80 mM Tris-borate (pH 8.3) and 1 mM EDTA for 3 h at 10 W constant power. The inositol polyphosphates were visualized by staining the gel with toluidine blue, as described above.

## Allelic replacement at the *siw14* locus

We constructed strains harboring marked *siw14*-WT and *siw14*-C189S alleles. First, we generated a pKS-based plasmid carrying a *siw14* integration cassette marked with *hygMX*. The cassette consisted of the following elements, proceeding from 5' to 3': (i) a 619-bp segment of genomic DNA 5' of the *siw14*<sup>+</sup> start codon; (ii) a 1107-bp segment encompassing the *siw14* ORF and introns; (iii) a 269-bp segment harboring the *nmt1*<sup>+</sup> transcription termination signal; (iv) a *hygMX* gene conferring resistance to hygromycin; and (v) a 748-bp segment of genomic DNA 3' of the *siw14*<sup>+</sup> stop codon. The integration cassette for *siw14*-C189S was generated by replacing a restriction fragment spanning the Cys189 codon in the wild-type integration cassette with a restriction fragment containing the C189S missense mutation. The *siw14* ORFs were sequenced to exclude the presence of unwanted mutations. The integration cassettes (WT and C189S) were excised from plasmids and transfected into haploid *S. pombe* cells. Hygromycin-resistant transformants were selected and analyzed by Southern blotting to verify marker integration at the *siw14* locus. The *siw14* ORFs in the *siw14*-WT-*hygMX* and *siw14*-C189S-*hygMX* strains were amplified by PCR and sequenced to confirm the *siw14* genotypes.

## Tests of mutational synergies

*siw14*Δ haploids were mixed on malt agar with haploids of the opposite mating type bearing differentially marked mutations in genes involved in inositol pyrophosphate metabolism (*asp1*, *aps1*) and inositol pyrophosphate sensing (*spx1*), RNA 3'-processing and Pol2 transcription termination (*ctf1*, *dis2*, *ppn1*, *swd22*, *ssu72*, *rhn1*), CTD prolyl isomerization (*pin1*), or pan-heptad mutations in the Pol2 CTD (*T4A*) to allow mating and sporulation. After affirming the presence of asci by microscopy and ensuing treatment with glusulase (which breaks down the ascus wall to release spores and kills any residual unmated vegetative cells), the spores were counted in a hemocytometer and then subjected to random spore analysis (34). Spores (~1,000) were plated in parallel on YES agar and on medium selective for the marked mutant alleles, and the plates were incubated at 30°C. A large number of viable drug-resistant progeny were screened by replica-plating for the presence of the second drug resistance marker gene or by sequentially replica-plating from YES to different drug-selective media. Wild-type (unmarked) and differentially marked single mutant alleles were recovered at the expected frequencies. A finding that no haploids with both marker genes were recovered after 6 to 8 days of incubation at 30°C was taken to indicate synthetic lethality. Growth phenotypes of viable double-mutant strains were assessed in parallel with the individual single mutants and wild-type cells at different temperatures (20°C to 37°C). Fission yeast cultures were grown in YES liquid medium at 30°C until A<sub>600</sub> reached 0.6–0.9. The cultures were adjusted to a final A<sub>600</sub> of 0.1, and 3 μL aliquots of serial fivefold dilutions were spotted on YES agar. The plates were photographed after incubation for 2 d at 34°C, 2.5 days at 30°C and 37°C, 4 days at 25°C, and 6 days at 20°C. A list of the fission yeast strains employed in this study is compiled in Table S4.

## Transcriptome profiling by RNA-seq

RNA was isolated from *S. pombe* wild-type and *siw14*Δ cells that were grown in liquid YES medium at 30°C to an A<sub>600</sub> of 0.5 to 0.6. Cells were harvested by centrifugation, and total RNA was extracted via the hot phenol method. The integrity of total RNA was gauged with an Agilent Technologies 2100 Bioanalyzer. The Illumina TruSeq stranded mRNA sample preparation kit was used to purify poly(A)<sup>+</sup> RNA from 500 ng of total RNA and to carry out the subsequent steps of poly(A)<sup>+</sup> RNA fragmentation, strand-specific cDNA synthesis, indexing, and amplification. Indexed libraries were normalized and pooled for paired-end sequencing performed using a NOVASeq 6000 system. FASTQ files bearing paired-end reads of length 51 bases were mapped to the *S. pombe* genome (ASM294v2.28) using HISAT2-2.1.0 with default parameters (35). The resulting SAM files were converted to BAM files using Samtools (36). Count files for individual replicates

were generated with HTSeq-0.10.0 (37) using exon annotations from Pombase (GFF annotations, genome-version ASM294v2; source “ensembl”). RPKM analysis and pairwise correlations (Tables S1 and S2) were performed as described previously (38). Differential gene expression and fold change analysis were performed in DESeq2 (39). The cutoff for further evaluation was set for genes that had an adjusted *P*-value (Benjamini-Hochberg corrected) of  $\leq 0.05$  and were up or down by at least twofold in *siw14Δ* versus wild type. Genes were further filtered on the following criteria: (i) genes that were  $\geq 2$ -fold up and the average normalized read count for the *siw14Δ* strain was  $\geq 100$  and (ii) genes that were  $\geq 2$ -fold down and the average normalized read count for the wild-type strain was  $\geq 100$ .

ACKNOWLEDGMENTS

This work was supported by the NIH grants R01-GM134021 (B.S.) and R35-GM126945 (S.S.) and by the German Research Foundation (DFG) under Germany's Excellence Strategy (CIBSS-EXC-2189-Project ID 390939984) (H.J.J.). A.M.S. is supported by NSF graduate research fellowship 1746057.

The authors declare that they have no conflicts of interest with the contents of this article.

AUTHOR AFFILIATIONS

- <sup>1</sup>Molecular Biology Program, Sloan Kettering Institute, New York, New York, USA
- <sup>2</sup>Gerstner Sloan Kettering Graduate School of Biomedical Sciences, New York, New York, USA
- <sup>3</sup>Department of Microbiology and Immunology, Weill Cornell Medical College, New York, New York, USA
- <sup>4</sup>Institute of Organic Chemistry and Centre for Integrative Biological Signaling Studies, University of Freiburg, Freiburg, Germany
- <sup>5</sup>Spemann Graduate School of Biology and Medicine, University of Freiburg, Freiburg, Germany

AUTHOR ORCID*s*

Stewart Shuman  <http://orcid.org/0000-0001-5034-6438>

FUNDING

Funder	Grant(s)	Author(s)
<a href="#">HHS   NIH   National Institute of General Medical Sciences (NIGMS)</a>	R35-GM126945	Stewart Shuman
<a href="#">HHS   NIH   National Institute of General Medical Sciences (NIGMS)</a>	R01-GM134021	Beate Schwer
<a href="#">National Science Foundation (NSF)</a>	1746057	Ana M. Sanchez
<a href="#">Deutsche Forschungsgemeinschaft (DFG)</a>	390939984	Henning J. Jessen

AUTHOR CONTRIBUTIONS

Ana M. Sanchez, Conceptualization, Investigation, Writing – review and editing | Beate Schwer, Conceptualization, Funding acquisition, Investigation, Writing – review and editing | Nikolaus Jork, Methodology, Resources | Henning J. Jessen, Methodology, Resources | Stewart Shuman, Conceptualization, Funding acquisition, Investigation, Writing – original draft

## DIRECT CONTRIBUTION

This article is a direct contribution from Stewart Shuman, a Fellow of the American Academy of Microbiology, who arranged for and secured reviews by Adolfo Saiardi, University College London, and Ronda J. Rolfes, Georgetown University.

## DATA AVAILABILITY

The RNA-seq data in this publication have been deposited in NCBI's Gene Expression Omnibus and are accessible through GEO Series accession number [GSE232247](https://www.ncbi.nlm.nih.gov/geo/query/acc.cgi?acc=GSE232247).

## ADDITIONAL FILES

The following material is available [online](#).

## Supplemental Material

**Supplemental figures and tables (mBio02056-23-s0001.pdf).** Tables S1, S2, S3, and S4. Figures S1 and S2.

## REFERENCES

1. Azevedo C, Saiardi A. 2017. Eukaryotic phosphate homeostasis: the Inositol pyrophosphate perspective. *Trends Biochem Sci* 42:219–231. <https://doi.org/10.1016/j.tibs.2016.10.008>
2. Wang H, Falck JR, Hall TMT, Shears SB. 2012. Structural basis for an inositol pyrophosphate kinase surmounting phosphate crowding. *Nat Chem Biol* 8:111–116. <https://doi.org/10.1038/nchembio.733>
3. Pascual-Ortiz M, Saiardi A, Walla E, Jakopiec V, Künzel NA, Span I, Vangala A, Fleig U. 2018. Asp1 bifunctional activity modulates spindle function via controlling cellular Inositol pyrophosphate levels in *Schizosaccharomyces pombe*. *Mol Cell Biol* 38:e00047-18. <https://doi.org/10.1128/MCB.00047-18>
4. Dollins DE, Bai W, Fridy PC, Otto JC, Neubauer JL, Gattis SG, Mehta KPM, York JD. 2020. Vip1 is a kinase and pyrophosphatase switch that regulates inositol diphosphate signaling. *Proc Natl Acad Sci USA* 117:9356–9364. <https://doi.org/10.1073/pnas.1908875117>
5. Benjamin B, Garg A, Jork N, Jessen HJ, Schwer B, Shuman S. 2022. Activities and structure-function analysis of fission yeast inositol pyrophosphate (IPP) kinase-pyrophosphatase Asp1 and its impact on regulation of *Pho1* gene expression. *mBio* 13:e0103422. <https://doi.org/10.1128/mbio.01034-22>
6. Zhu J, Lau K, Puschmann R, Harmel RK, Zhang Y, Pries V, Gaugler P, Broger L, Dutta AK, Jessen HJ, Schaaf G, Fernie AR, Hothorn LA, Fiedler D, Hothorn M. 2019. Two bifunctional inositol pyrophosphate kinases/phosphatases control plant phosphate homeostasis. *Elife* 8:e43582. <https://doi.org/10.7554/eLife.43582>
7. Gu C, Nguyen HN, Hofer A, Jessen HJ, Dai X, Wang H, Shears SB. 2017. The significance of the bifunctional kinase/phosphatase activities of diphosphoinositol pentakisphosphate kinases (PIPKs) for coupling inositol pyrophosphate cell signaling to cellular phosphate homeostasis. *J Biol Chem* 292:4544–4555. <https://doi.org/10.1074/jbc.M116.765743>
8. Randall TA, Gu C, Wang H, Shears SB. 2020. A two-way switch for Inositol pyrophosphate signaling: evolutionary history and biological significance of a unique, bifunctional kinase/phosphatase. *Adv Biol Regul* 75:100674. <https://doi.org/10.1016/j.jbior.2019.100674>
9. Safrany ST, Caffrey JJ, Yang X, Bembenek ME, Moyer MB, Burkhart WA, Shears SB. 1998. A novel context for the 'Mutt' module, a guardian of cell integrity, in a diphosphoinositol polyphosphate phosphohydrolase. *EMBO J* 17:6599–6607. <https://doi.org/10.1093/emboj/17.22.6599>
10. Safrany ST, Ingram SW, Cartwright JL, Falck JR, McLennan AG, Barnes LD, Shears SB. 1999. The diadenosine hexaphosphate hydrolase from *Schizosaccharomyces pombe* and *Saccharomyces cerevisiae* are homologues of the human diphosphoinositol polyphosphate phosphohydrolase: overlapping substrate specificities in a MutT-type protein. *J Biol Chem* 274:21735–21740. <https://doi.org/10.1074/jbc.274.31.21735>
11. Kilari RS, Weaver JD, Shears SB, Safrany ST. 2013. Understanding inositol pyrophosphate metabolism and function: kinetic characterization of the diphosphatase. *FEBS Lett* 587:3464–3470. <https://doi.org/10.1016/j.febslet.2013.08.035>
12. Zong G, Jork N, Hostachy S, Fiedler D, Jessen HJ, Shears SB, Wang H. 2021. New structural insights reveal an expanded reaction cycle for inositol pyrophosphate hydrolysis by human DIPPI. *FASEB J* 35:e21275. <https://doi.org/10.1096/fj.202001489R>
13. Yang X, Safrany ST, Shears SB. 1999. Site-directed mutagenesis of diphosphoinositol polyphosphate phosphohydrolase, a dual specificity NUDT enzyme that attacks diadenosine polyphosphates and diphosphoinositol polyphosphates. *J Biol Chem* 274:35434–35440. <https://doi.org/10.1074/jbc.274.50.35434>
14. Lonetti A, Szigyarto Z, Bosch D, Loss O, Azevedo C, Saiardi A. 2011. Identification of an evolutionarily conserved family of inorganic polyphosphate endopolyphosphatases. *J Biol Chem* 286:31966–31974. <https://doi.org/10.1074/jbc.M111.266320>
15. Márquez-Moñino MÁ, Ortega-García R, Shipton ML, Franco-Echevarría E, Riley AM, Sanz-Aparicio J, Potter BVL, González B. 2021. Multiple substrate recognition by yeast diadenosine and diphosphoinositol polyphosphate phosphohydrolase through phosphate clamping. *Sci Adv* 7:eabf6744. <https://doi.org/10.1126/sciadv.abf6744>
16. Steidle EA, Chong LS, Wu M, Crooke E, Fiedler D, Resnick AC, Rolfes RJ. 2016. A novel inositol pyrophosphate phosphatase in *Saccharomyces cerevisiae*: the *siw14* protein selectively cleaves the B-phosphate from 5-diphosphoinositol pentakisphosphate (5Pp-IP5). *J Biol Chem* 291:6772–6783. <https://doi.org/10.1074/jbc.M116.714907>
17. Wang H, Gu C, Rolfes RJ, Jessen HJ, Shears S. 2018. Structural and biochemical characterization of *siw14*: a protein-tyrosine phosphatase fold that metabolizes inositol pyrophosphates. *J Biol Chem* 293:6905–6914. <https://doi.org/10.1074/jbc.RA117.001670>
18. Florio TJ, Lokareddy RK, Gillilan RE, Cingolani G. 2019. Molecular architecture of the inositol phosphatase *siw14*. *Biochem* 58:534–545. <https://doi.org/10.1021/acs.biochem.8b01044>
19. Gaugler P, Schneider R, Liu G, Qiu D, Weber J, Schmid J, Jork N, Häner M, Ritter K, Fernández-Rebollo N, Giehl RF, Trung MN, Yadav R, Fiedler D, Gaugler V, Jessen HJ, Schaaf G, Laha D. 2022. Arabidopsis PFA-DSP-type phosphohydrolases target specific inositol pyrophosphate messengers. *Biochem* 61:1213–1227. <https://doi.org/10.1021/acs.biochem.2c00145>
20. Wang H, Perera L, Jork N, Zong G, Riley AM, Potter BV, Jessen HJ, Shears SB. 2022. A structural exposé of noncanonical molecular reactivity within the protein tyrosine phosphatase WPD loop. *Nat Commun* 13:2231. <https://doi.org/10.1038/s41467-022-29673-y>
21. Sanchez AM, Garg A, Shuman S, Schwer B. 2019. Inositol pyrophosphates impact phosphate homeostasis via modulation of RNA 3'

- processing and transcription termination. *Nucleic Acids Res* 47:8452–8469. <https://doi.org/10.1093/nar/gkz567>
22. Garg A, Shuman S, Schwer B. 2020. A genetic screen for suppressors of hyper-repression of the fission yeast *PHO* regulon by Pol2 CTD mutation T4A implicates inositol 1-pyrophosphates as agonists of precocious IncRNA transcription termination. *Nucleic Acids Res* 48:10739–10752. <https://doi.org/10.1093/nar/gkaa776>
  23. Garg A, Shuman S, Schwer B. 2022. Genetic screen for suppression of transcriptional interference reveals fission yeast 14-3-3 protein Rad24 as an antagonist of precocious Pol2 transcription termination. *Nucleic Acids Res* 50:803–819. <https://doi.org/10.1093/nar/gkab1263>
  24. Schwer B, Garg A, Sanchez AM, Bernstein MA, Benjamin B, Shuman S. 2022. Cleavage-polyadenylation factor Cft1 and SPX domain proteins are agents of inositol pyrophosphate toxicosis in fission yeast. *mBio* 13:e0347621. <https://doi.org/10.1128/mbio.03476-21>
  25. Sanchez AM, Garg A, Schwer B, Shuman S. 2023. Duf89 abets incRNA control of fission yeast phosphate homeostasis via its antagonism of precocious incRNA transcription termination. *RNA* 29:808–825. <https://doi.org/10.1261/rna.079595.123>
  26. Gerasimaitė R, Sharma S, Desfougères Y, Schmidt A, Mayer A. 2014. Coupled synthesis and translocation restrains polyphosphate to acidocalcisome-like vacuoles and prevents its toxicity. *J Cell Sci* 127:5093–5104. <https://doi.org/10.1242/jcs.159772>
  27. Vanoosthuysen V, Legros P, van der Sar SJ, Yvert G, Toda K, Le Bihan T, Watanabe Y, Hardwick K, Bernard P. 2014. CPF-associated phosphatase activity opposes condensin-mediated chromosome condensation. *PLoS Genet* 10:e1004415. <https://doi.org/10.1371/journal.pgen.1004415>
  28. Jasnovidova O, Krejčíková M, Kubicek K, Stefl R. 2017. Structural insight into recognition of phosphorylated threonine-4 of RNA polymerase II C-terminal domain by Rtt103P. *EMBO Rep* 18:906–913. <https://doi.org/10.15252/embr.201643723>
  29. Sanchez AM, Garg A, Shuman S, Schwer B. 2020. Genetic interactions and transcriptomics implicate fission yeast CTD prolyl isomerase pin1 as an agent of RNA 3' processing and transcription termination that functions via its effects on CTD phosphatase ssu72. *Nucleic Acids Res* 48:4811–4826. <https://doi.org/10.1093/nar/gkaa212>
  30. Sanchez AM, Shuman S, Schwer B. 2018. RNA polymerase II CTD interactome with 3' processing and termination factors in fission yeast and its impact on phosphate homeostasis. *Proc Natl Acad Sci USA* 115:E10652–E10661. <https://doi.org/10.1073/pnas.1810711115>
  31. Zhang ZY, Clemens JC, Schubert HL, Stuckey JA, Fischer MW, Hume DM, Saper MA, Dixon JE. 1992. Expression, purification, and physicochemical characterization of a recombinant yersinia protein tyrosine phosphatase. *J Biol Chem* 267:23759–23766. <https://doi.org/https://www.sciencedirect.com/science/article/pii/S0021925818359039?via%3Dihub>
  32. Zhang ZY, Dixon JE. 1993. Active site labeling of the *Yersinia* protein tyrosine phosphatase: the determination of the pK<sub>a</sub> of the active site cysteine and the function of the conserved histidine 402. *Biochem* 32:9340–9345. <https://doi.org/10.1021/bi00087a012>
  33. Auesukaree C, Homma T, Tochio H, Shirakawa M, Kaneko Y, Harashima S. 2004. Intracellular phosphate serves as a signal for the regulation of the PHO pathway in *Saccharomyces cerevisiae*. *J Biol Chem* 279:17289–17294. <https://doi.org/10.1074/jbc.M312202200>
  34. Escorcia W, Forsburg SL. 2018. Random spore analysis in fission yeast. *Methods Mol Biol* 1721:189–195. [https://doi.org/10.1007/978-1-4939-7546-4\\_17](https://doi.org/10.1007/978-1-4939-7546-4_17)
  35. Kim D, Langmead B, Salzberg SL. 2015. HISAT: a fast spliced aligner with low memory requirements. *Nat Methods* 12:357–360. <https://doi.org/10.1038/nmeth.3317>
  36. Li H, Handsaker B, Wysoker A, Fennell T, Ruan J, Homer N, Marth G, Abecasis G, Durbin R. 2009. The sequence alignment/map format and SAMtools. *Bioinf* 25:2078–2079. <https://doi.org/10.1093/bioinformatics/btp352>
  37. Anders S, Pyl PT, Huber W. 2015. HTSeq—a python framework to work with high-throughput sequencing data. *Bioinf* 31:166–169. <https://doi.org/10.1093/bioinformatics/btu638>
  38. Schwer B, Bitton DA, Sanchez AM, Bähler J, Shuman S. 2014. Individual letters of the RNA polymerase II CTD code govern distinct gene expression programs in fission yeast. *Proc Natl Acad Sci USA* 111:4185–4190. <https://doi.org/10.1073/pnas.1321842111>
  39. Love MI, Huber W, Anders S. 2014. Moderated estimation of fold change and dispersion for RNA-seq data with DESeq2. *Genome Biol* 15:550. <https://doi.org/10.1186/s13059-014-0550-8>